Solvation of Coumarin 314 at Water/Air Interfaces Containing Anionic Surfactants. I. Low Coverage

Diego A. Pantano,[†] Milton T. Sonoda,[‡] Munir S. Skaf,[‡] and Daniel Laria*,[†,§]

Departamento de Química Inorgánica, Analítica y Química-Física e INQUIMAE, Facultad de Ciencias Exactas y Naturales, Universidad de Buenos Aires, Ciudad Universitaria, Pabellón II, 1428 Buenos Aires, Argentina, Instituto de Química, Universidade Estadual de Campinas, Cx. P. 6154, Campinas, SP 13083-970, Brazil, and Unidad Actividad Química, Comisión Nacional de Energía Atómica, Avenida Libertador 8250, 1429 Buenos Aires, Argentina

Through the use of molecular dynamics techniques, we analyze equilibrium and dynamical aspects of the solvation of Coumarin 314 adsorbed at water/air interfaces in the presence of sodium dodecyl sulfate surfactant molecules. Three different coverages in the submonolayer regime were considered, 500, 250, and 100 Å^2/SDS molecule. The surfactant promotes two well-differentiated solvation environments, which can be clearly distinguished in terms of their structures for the largest surfactant coverage considered. The first one is characterized by the probe lying adjacent or exterior to two-dimensional spatial domains formed by clustered surfactant molecules. A second type of solvation environment is found in which the coumarin appears embedded within compact surfactant domains. Equilibrium and dynamical aspects of the interfacial orientation of the probe are investigated. Our results show a gradual transition from parallel to perpendicular dipolar alignment of the probe with respect to the interface as the concentration of surfactant ρ_s increases. The presence of the surfactant leads to an increase in the roughness and in the characteristic width of the water/air interface. These modifications are also manifested by the decorrelation times for the probe reorientational dynamics, which become progressively slower with ρ_s in both solvation states, although much more pronounced for the embedded ones. The dynamical characteristics of the solvation responses of the charged interfaces are also analyzed, and the implications of our findings to the interpretation of available experimental measurements are discussed.

I. Introduction

Liquid−vapor interfaces constitute nonuniform environments where most variables controlling chemical reactivity present abrupt changes over length scales comparable to typical molecular sizes. These sharp gradients open new interesting scenarios, where reaction mechanisms are well-differentiated from what is normally encountered in bulk liquid or gaseous isotropic phases.[1−3] Clear manifestations of these phenomena can be found in displacements of chemical equilibria,[4] in modifications of rates and mechanisms[5] of surface reactions, and in local enhancements of pH,[6] to list just a few important examples. In all of these cases, interfacial solvation plays a fundamental role.

Most of the direct experimental information about solvation dynamics in condensed phases is obtained through signals from molecular probes; among which, coumarins stand out as a group of versatile solvatochromic dyes commonly used in steady-state and time-resolved fluorescence spectroscopy. Without being exhaustive, the list of different environments that have been investigated using these probes includes polar[7] and nonpolar[8] homogeneous liquid phases and inhomogeneous environments, such as nanoclusters,[9,10] self-assembled structures,[11] and interfaces.[12−22] Microscopic descriptions related to equilibrium solvation structures and solvent dynamics are essential for the correct interpretation of the chemical reactivity characteristics prevailing in each specific environment.

The study of surfactant-coated, charged interfaces has received considerable attention in recent times.[18,23−27] The interest in these systems resides mainly in the fact that charged interfaces may incorporate the basic functional and structural groups that allow for the stabilization of more complex supramolecular assemblies of biological interest, such as micelles, lipidic bilayers, and cell membranes. The presence of adsorbed ionic surfactant introduces new characteristics to the solvation structures found at bare interfaces. Most notable are those associated with the strong local electric fields created by the surfactant headgroups and counterions. In many cases, the resulting electrostatic coupling between the chemical species at the interface may be significant in comparison to that involved in a typical aqueous hydrogen bond. Therefore, it is reasonable to expect alterations in the−already modified with respect to bulk phases−intermolecular connectivity and orientational correlations of interfacial water. The presence of charged species also affects the interfacial dynamics in important ways. The main physical effect promoted by the surfactant electric fields is the overall slowing down of the dynamical modes of the water molecules in close contact with the surfactant.[28]

In this work, we investigate equilibrium and dynamical aspects of the solvation of dyes adsorbed at charged liquid/air interfaces. More specifically, we report results from molecular

* Author to whom correspondence should be addressed. E-mail: dhlaria@cnea.gov.ar.
[†] Universidad de Buenos Aires.
[‡] Universidade Estadual de Campinas.
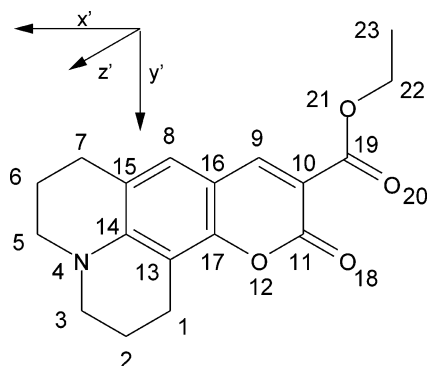[§] Comisión Nacional de Energía Atómica.

Figure 1. Coumarin 314 molecular structure and labeling.

dynamics (MD) computer experiments performed on model systems consisting of a Coumarin 314 (C314) molecule (Figure 1) lying at water/air interfaces in the presence of different concentrations of the anionic surfactant sodium dodecyl sulfate (SDS). This study is largely motivated by recent time-resolved second harmonic generation[29] (TRSHG) spectroscopy measurements performed on these systems by Benderskii and Eisenthal.[23] It has been found that the diffusive component of the TRSHG solvation response is described by a biexponential decay in which the corresponding characteristic times exhibit a complex dependence on the degree of surfactant coverage (i.e., the surface charge density). At very low (500 Å^2/SDS molecule) and intermediate (250 Å^2/SDS molecule) surface coverages, the fast components of the measured responses remain similar to those found for the bare interface ($\tau_1 \approx 250$ fs) and bulk water ($\sim$130−250 fs) but slow to 600 fs at higher coverages (100 Å^2/SDS molecule). The slower component of the solvation response, however, changes from $\tau_2 = 2.0$ ps for bare interfaces to nearly 4.4 ps at the lowest sulfate surface coverage considered (500 Å^2/SDS molecule) and to 5.4 ps at 100 Å^2/SDS molecule.

The complex behavior displayed by the solvation dynamics at such charged surfaces is far from being understood. In particular, the solvent dynamics underlying the relaxation components are unknown. Benderskii and Eisenthal have proposed a correspondence between the experimental TRSHG time scales and two microscopic features involving the interfacial water molecules, the enhancement in the hydrogen bonding network connectivity and modifications of the dynamical modes. In an effort to provide additional information from a molecular perspective, we present simulation results showing evidence that, in addition to the above-mentioned effects, the interfacial solvation dynamics of C314 are also affected in a sensible fashion by the different solvation environments generated by the surfactant spatial domains. The systems we consider here correspond to surfaces below the full-monolayer surfactant coverage ($\geq$100 Å^2/SDS molecule) and represent a natural extension of our recent work on the solvation of similar probes at clean interfaces.[30] Yet, the present simulations reveal interesting new features of the dynamics at the interface, which may have implications for the interpretation of the experimental data. In particular, we find that the interfacial solvation of the C314 molecule exhibits two predominant types of structures, those in which the C314 molecule sits at the edge of a two-dimensional surfactant spatial domain and those where the solute probe sits in the interior of a surfactant patch. The interconversion between these two types of solvation environments and the overall dynamics of the probe itself constitute important aspects of the simulated solvation dynamics.

This paper is organized as follows. Details of the simulation procedure and models are described in section II. The main

results and discussion are presented in section III. Our concluding remarks appear in section IV.

II. Model and Simulation Procedure

The MD experiments described in this paper were performed on systems composed of a C314 molecule lying at one of the liquid/air interfaces of an aqueous slab comprising $N_w = 1000$ water molecules. The slab was generated from a fully periodic, cubic system of density 1 g cm^{-3}, in which periodic boundary conditions were suppressed along one of the main axes of the simulation box (hereafter referred to as the z-axis). After an initial equilibration period of 100 ps, equal numbers N_s of dodecyl sulfate [CH$_3$(CH$_2$)$_{11}$OSO$_3$]$^-$ and Na$^+$ counterions were distributed across the interface containing the C314. The initial intramolecular arrangement of the surfactant molecules corresponded to that of a fully trans conformer, with their head-to-tail vectors oriented perpendicularly to the surface. Three different surface coverages were considered, $N_s = 2$, 5, and 10, which expressed in terms of the overall interfacial density, ρ_s, correspond roughly to $\rho_s = 0.002$, 0.005, and 0.01 Å^{-2}, respectively. This density regime is below the estimated value for the saturated monolayer,[31] $\rho_s \approx 1.25 \times 10^{-2}$ Å^{-2} and was chosen so as to coincide with available experimental information under similar conditions.[23]

Water molecules and the chromophore were modeled as rigid bodies containing a collection of interaction sites. For the water molecules, we adopted the simple point charge (SPC) model.[32] Charge distributions for the C314 ground and first excited electronic states and molecular geometry were identical to the ones we considered previously,[30] which were obtained from the AM1 semiempirical parametrization using the AMPAC package.[33−36] Within this level of description, the C314 dipole moment in the ground state is $\mu = 8.4$ D, in reasonable agreement to the experimental value (8.20 ± 0.02 D).[37] A complete description of the partial charges and the molecular geometry of the dye is provided in ref 30. For the surfactant, we used the fully flexible model proposed by Dominguez et al.[25] Each surfactant comprises a total of 17 interaction sites, using the united atom description for CH$_2$ and CH$_3$ groups. Intramolecular interactions include stretching, bending, and dihedral contributions. Additional details of the surfactant molecules and the atomic parameters for the counterions can be obtained from ref 25.

We implemented a MD scheme that included a reversible multiple time step algorithm to integrate Newton's equation of motion. The dynamical trajectories corresponded to microcanonical runs at temperatures close to $T \approx 298$ K. In this temperature regime, all slabs presented stable structures, with negligible evaporation. After initial equilibration runs of typically $\sim$500 ps, statistics were collected along equilibrium trajectories of $\sim$3−5 ns. Two different time steps were used, $\Delta t = 1$ fs for the intermolecular motions and $\delta t = \Delta t/3$ to evolve the rest of the fast dynamical variables associated to the surfactant internal degrees of freedom. Intramolecular constraints in water and C314 were handled using the RATTLE algorithm.[38] All interactions were truncated at $R_c = 15.5$ Å and brought to zero in an interval of 1 Å by a fourth-degree spline.[39]

III. Results and Discussion

A. Slab Structures. The starting point of our analysis will be the consideration of a set of density fields associated with the relevant chemical species. For purposes of clarity, water molecules will be referred to as "solvent", whereas the term "solute" will be used to indistinctly denote the rest of the chemical species. We first focus our attention on two different
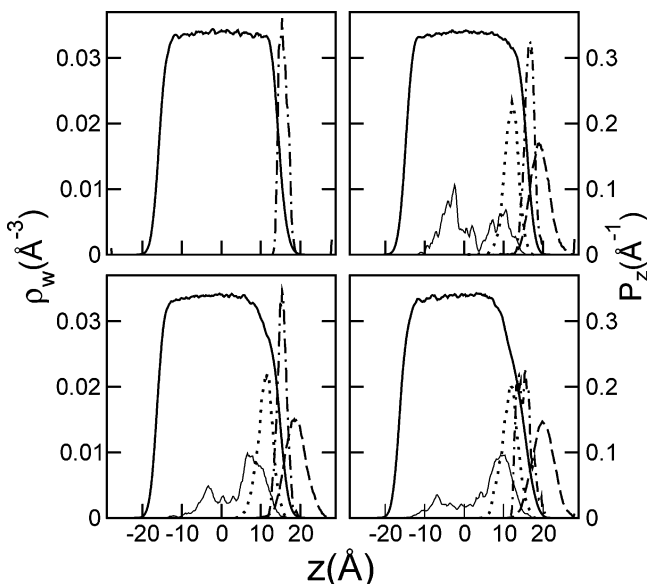
Solvation of Coumarin 314 at Water/Air Interfaces

J. Phys. Chem. B, Vol. 109, No. 15, 2005 **7367**

Figure 2. Water local density (thick solid lines, left axis) and probability densities (right axis) for different solute species along directions perpendicular to the interface: C314 center of mass (dot−dashed lines); counterions (thin solid lines); S (dotted lines); CH₃ (dashed lines). Top-left panel, bare interfaces; top-right panel, ρ_s = 0.002 Å⁻²; bottom-left panel, ρ_s = 0.005 Å⁻²; bottom-right panel, ρ_s = 0.01 Å⁻².

kinds of spatial correlations. (i) For the solvent, we have computed $\rho_w(z)$ dz, the number of water molecules per unit of area in the xy plane, A, with their centers of mass lying between z and z + dz

$$\rho_w(z) = \frac{1}{A}\langle \sum_{i=1}^{N_w} \delta(Z_i - Z_{CM} - z)\rangle \qquad (1)$$

In this equation, $\langle \cdots \rangle$ denotes an equilibrium ensemble average; Z_i and Z_{CM} represent the z-coordinates of the centers of mass of the ith water molecule and the water slab, respectively. (ii) For the solute species, we consider spatial correlations of the type

$$P_\alpha(z) = \frac{1}{N_\alpha}\langle \sum_{i=1}^{N_\alpha} \delta(z_i^\alpha - Z_{CM} - z)\rangle \qquad (2)$$

where z_i^α represents the z-coordinate of the α site in the ith molecule (i = 1, 2, ..., N_α). Densities of four selected solute species were examined, the Na⁺ counterions, the center of mass of the C314 molecule, and two distal surfactant sites, namely, the S atom in the headgroup and the terminal CH₃ group in the hydrophobic aliphatic tail.

Results for spatial correlation functions in different charged interfaces are shown in Figure 2, which also includes results for C314 adsorbed at bare interfaces as a reference benchmark. Results for $\rho_w(z)$ show that the four aqueous slabs present similar widths, $\Delta L \approx$ 31 Å, measured from the positions of the two Gibbs dividing surfaces. Charge localization on the right-hand side interfaces promotes a barely discernible enhancement of the water local density, as one gradually moves from the negative to the positive portion of the z-axis. However, all average water densities at the middle points of the slabs fall within the interval $\rho_w(z = 0) = 0.034 \pm 0.001$ Å⁻³, which is in close agreement to the bulk water density at ambient conditions, $\rho_b = 0.0334$ Å⁻³.
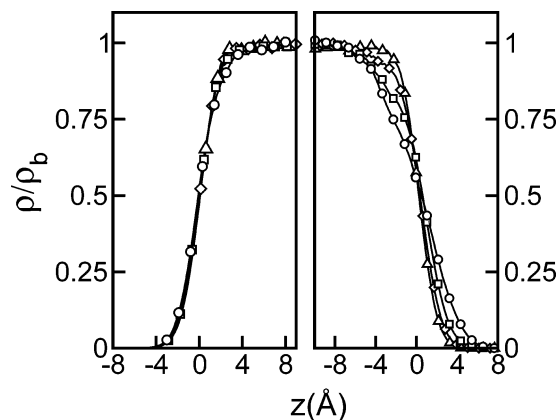

Figure 3. Local water density in the vicinity of the Gibbs dividing surfaces for bare (left panel) and charged (right panel) interfaces. Circles, $\rho_s = 0.01$ Å⁻²; squares, $\rho_s = 0.005$ Å⁻²; diamonds, $\rho_s = 0.002$ Å⁻²; triangles, bare interface. The origins of the z-axis coincide with the positions of the corresponding Gibbs dividing surfaces.

The degree of penetration of the C314 center of mass into the water slabs remains practically unchanged at low surfactant coverages, and only for $\rho_s = 0.01$ Å⁻², one observes a mild shift in the position of the probe toward the interior of the aqueous phase (from $z \approx 17$ Å down to ~15 Å). At this surface coverage, one can also notice somewhat larger fluctuations in the probability distribution functions. These changes go hand-in-hand with an increase in the characteristic length scale that describes the width of the interface, $\mathcal{L}$. The direct comparison between $\rho_w(z)$ for clean and charged interfaces shown in Figure 3 is instructive. All profiles are practically identical on the surfactant-free side (left panel), whereas for charged interfaces (right panel), $\rho_w(z)$ presents a gradual widening as the density of surface charge increases. To acquire a quantitative idea of this effect, we took the z-coordinates at 10% and 90% of the maximum density value to compute the width for the largest surfactant coverage, $\mathcal{L}(\rho_s = 0.01$ Å⁻²$) \approx 8.2$ Å. This width is approximately twice that of the bare interface, $\mathcal{L} \approx 3.6$ Å.

In the concentration range considered, the penetration of the polar headgroups into the aqueous phase is found to be somewhat deeper in comparison to the coumarin ($z \approx 11-12$ Å), while the average positions of the distal CH₃ groups were found to be approximately at $\Delta z \approx 7-8$ Å outward. These structures are accordant to that reported for the case of infinitely diluted SDS.[25] From the average positions of the distal groups of the surfactant molecules (S and CH₃), it is possible to get a crude estimate of the overall orientation of the amphiphiles at the surface. Considering a typical head-to-tail length of $L_s \approx 15$ Å, one can estimate the overall orientation θ_s of the surfactant tails with respect to the z-axis as $\theta_s \approx \cos^{-1}(\Delta z/L_s) \approx 60°$. This shows that in this regime of surface coverage, the hydrophobic tails still lie close to the aqueous interface. In all cases, the distributions of couterions present two peaks. The inner ones, located near the center of the aqueous phase, $z \approx -5$ Å, correspond to "bulk" solvated ions, while the most prominent ones are located at typical values $z \approx 9-10$ Å. This particular structure is the combined result of the attraction exerted by the adsorbed polar heads—generating both, contact and solvent separated, Na⁺−SO₃⁻ ion pairs—and the cation avoidance of the bare liquid/vapor (surfactant free) interface.[43]

B. Coumarin Interfacial States. Having established the main structural features of the different slabs, we will now proceed to the microscopic characteristics of the interfacial solvation environments. We will first examine orientational correlations. To facilitate the description, it is convenient to define a local
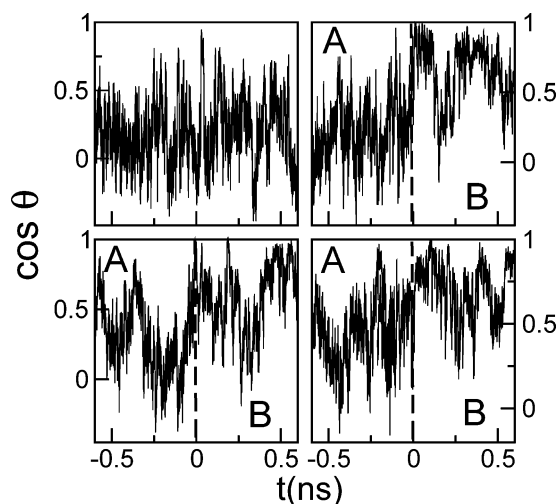
Figure 4. Temporal evolution of the out-of-plane orientation of Coumarin 314 adsorbed at different charged water/air interfaces. Top-left panel, bare interface; top-right panel, $\rho_s = 0.002$ Å^{-2}; bottom-left panel, $\rho_s = 0.005$ Å^{-2}; bottom-right panel, $\rho_s = 0.01$ Å^{-2}. The trajectories were time-aligned so that transitions between solvation states $\mathcal{A}$ and $\mathcal{B}$ take place at approximately $t = 0$

Figure 5. Probability distributions for the out-of-plane orientation for adsorbed Coumarin 314 for solvation states $\mathcal{A}$ (solid lines) and $\mathcal{B}$ (dashed lines) at different surfactant concentrations. (a) Bare interface; (b) $\rho_s = 0.005$ Å^{-2}; (c) $\rho_s = 0.002$ Å^{-2}; (d) $\rho_s = 0.01$ Å^{-2}.

system of coordinates (x', y', z'), as shown in Figure 1. Note that, in this frame, the atomic coordinates of the probe lie mostly on the $z' = 0$ plane, while the molecular dipole moment makes an angle of 18° with the x' direction. Previous simulation studies have shown that, in the absence of surfactant, the plane of the coumarin remains mostly parallel to the interface.[30]

Figure 4 includes details of the time evolution of the angular variable related to the out-of-plane dynamics of the probe, namely

$$\cos \theta(t) = \hat{\boldsymbol{\mu}}(t) \cdot \hat{\mathbf{z}} \qquad (3)$$

for charged and uncharged interfaces. The results for the latter (top-left panel) are practically identical to those presented in our previous study[30] and are accordant to the value reported in ref 15 obtained from null-angle, SHG experiments,[44] $\cos \theta \approx 0.17$. The prevalence of positive values for $\cos \theta$ in most of the trajectories indicates a moderate preferential solvation of the negatively charged end of the probe.

Orientational correlations at charged interfaces contrast sharply with the previous picture. The three trajectories present two well-differentiated temporal domains. During the first segments (hereafter denoted as states $\mathcal{A}$), and specially at low surfactant coverage, the time history of $\cos \theta(t)$ closely resembles the one already described for bare interfaces, namely, moderate orientation fluctuations with $\cos \theta$ typically between approximately -0.2 and 0.5. Sudden transitions take place at $t = 0$ when the values of $\cos \theta$ increase abruptly, suggesting a stronger alignment of the coumarin dipole along directions perpendicular to the interface. These configurations will be hereafter denoted as states $\mathcal{B}$. Differences between states $\mathcal{A}$ and $\mathcal{B}$, as reflected from the orientation of the probe, become even more evident from the inspection of the distributions depicted in Figure 5 for the quantity

$$P_{\mathcal{O}}(\cos \theta_0) = \langle \delta(\cos \theta - \cos \theta_0) \rangle_{\mathcal{O}} \qquad (4)$$

where $\langle \cdots \rangle_{\mathcal{O}}$ represents a restricted time average for episodes of type $\mathcal{O} = \mathcal{A}, \mathcal{B}$. Note that, as ρ_s increases, there is a gradual tendency toward perpendicular alignment of the C314 molecular plane with respect to the interface normal and a considerable reduction in the size of the corresponding fluctuations.
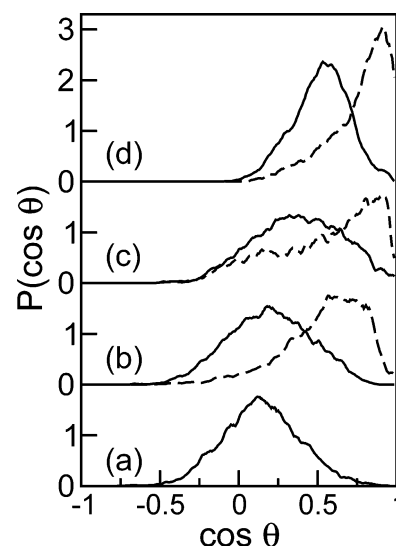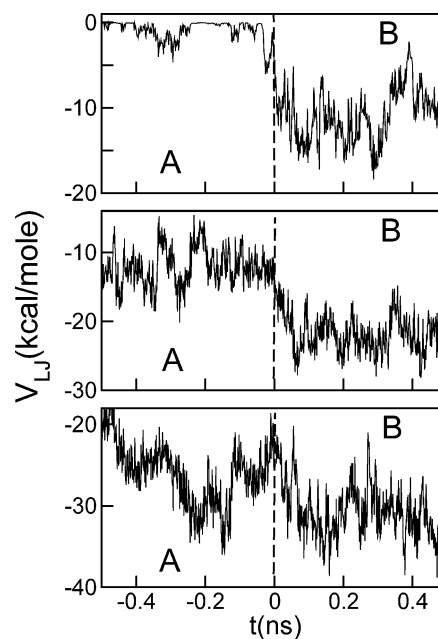

Figure 6. Time evolution of the Lennard-Jones contributions to the surfactant−coumarin coupling for different surfactant concentrations. Top panel, $\rho_s = 0.005$ Å^{-2}; middle panel, $\rho_s = 0.002$ Å^{-2}; lower panel, $\rho_s = 0.01$ Å^{-2}.

A similar description, but based on energetic grounds, can also be readily obtained by monitoring the coupling between the probe and the surfactant molecules. The most clear example is provided by V_{LJ}, the Lennard-Jones contribution to that coupling, whose time evolution in shown in Figure 6. Through the use of this energetic order parameter, one observes that smaller C314−surfactant LJ couplings are involved in states of type $\mathcal{A}$. The overall analysis of these observations suggests that a distinctive signature to differentiate these two states is likely to be found in modifications of the solvation structure provided by the SDS hosting of the probe.

To shed light on this point, it will be instructive to pause for a moment to establish a clearer distinction between the types of surface environments associated with states $\mathcal{A}$ and $\mathcal{B}$. Typical snapshots of configurations for states $\mathcal{A}$ and $\mathcal{B}$ for the largest
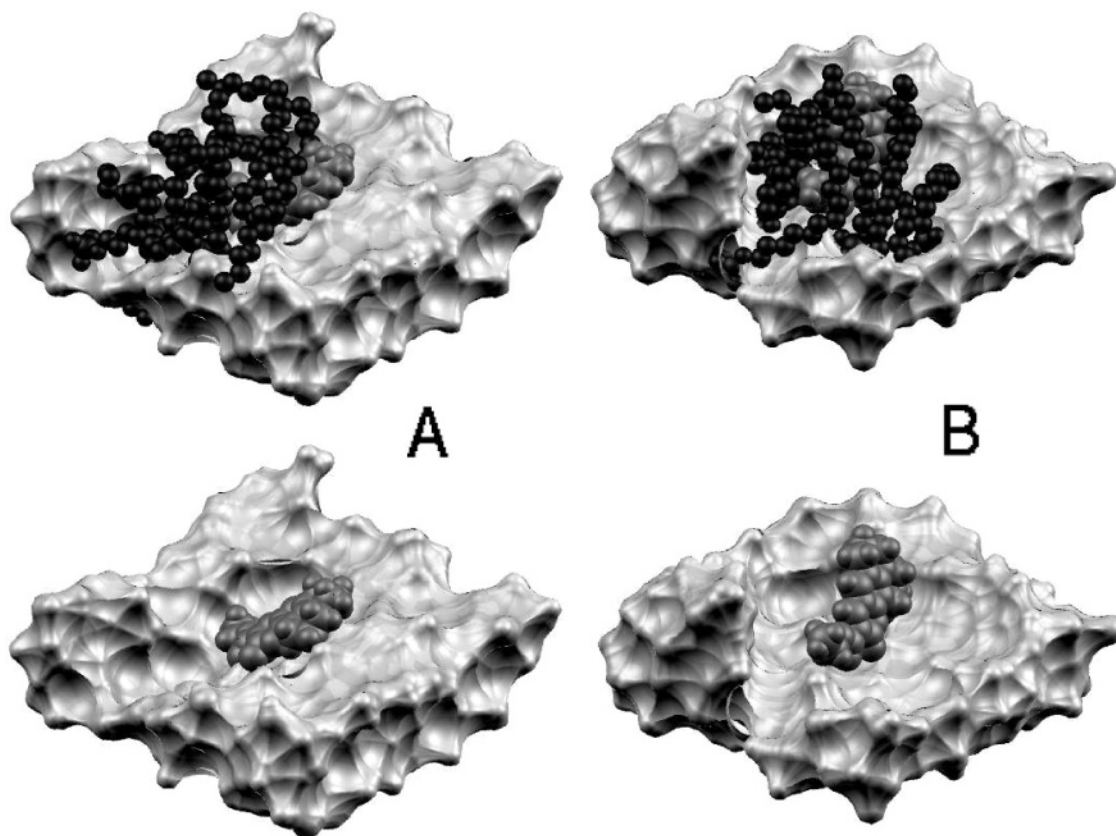
Solvation of Coumarin 314 at Water/Air Interfaces

J. Phys. Chem. B, Vol. 109, No. 15, 2005 **7369**

Figure 7. Top, snapshots of solvation states $\mathscr{A}$ and $\mathscr{B}$. Surfactants, Coumarin 314 and water are rendered in black, dark gray, and light gray, respectively. No atomistic details are depicted in the aqueous phase. Bottom, same as top figures with the surfactant omitted.

surfactant concentration analyzed are shown in Figure 7. The main differences are self-evident. In states $\mathscr{A}$, the coumarin appears external or adjacent to a two-dimensional spatial domain formed by a clustered group of SDS molecules. For states $\mathscr{B}$, however, the coumarin appears completely surrounded ("solvated") by the SDS molecules within one of these two-dimensional domains. Such a molecular view allows a sensible physical interpretation for the C314 average orientation relative to the surface that we have discussed above. Namely, in the compact surfactant structure $\mathscr{B}$, the C314 aligns perpendicular to the surface, and there is a reduction of the contact area with the aqueous substrate. Conversely, a direct inspection of a large series of configurations for solvation states of type $\mathscr{A}$ at high surfactant concentrations showed that, despite the propensity toward perpendicular alignment, the probe maintains close contact with the aqueous phase. This is made possible via a local enhancement of the roughness of the water surface, which we have already referred to in connection to the widths $\mathscr{L}$ shown in Figure 3. Incidentally, the degree of the surface roughness can be clearly visualized from the snapshots in the lower portion of Figure 7, where the surfactants have been omitted for purposes of clarity.

Several important conclusions can be drawn from the analyses carried out so far. First, the characteristics of the two solvation environments and the mechanisms that drive the interconversions between them will be intimately connected to those governing local interfacial concentration fluctuations of the surfactant. Second, packing effects within the surfactant domains lead to larger values of cos θ and to a lesser extent of the corresponding orientational fluctuations in states of type $\mathscr{B}$. Third, in terms of the dynamics, one observes that spontaneous transitions between the two solvation states for the adsorbed C314 take place at least in the nanosecond time scale or even longer.

Given these scenarios, it is clear that a rigorous analysis of the resulting distribution of surfactant cluster sizes and the interconversion dynamics between these structures for different values of ρ_s are well beyond the scope of the present study. Limitations in the largest length scale accessible in the present simulations as well as in the maximum number of particles preclude an adequate treatment of all relevant surfactant density fluctuations. Besides, although in the course of a typical $\sim$5 ns trajectory we did observe several $\mathscr{A}-\mathscr{B}$ transitions in both directions, the magnitudes of the time scales governing concentration fluctuations for surfactant species were comparable to the total length of our simulation runs. In view of these restrictions, we have not proceeded any further in these directions. Nevertheless, we still believe that, based on the previous observations, that the following physical picture holds. At low SDS concentrations, the degree of surface coverage is sufficiently low to allow for large fluctuations in the local, two-dimensional surfactant density fields. This would promote a distribution of energetically favorable clustering of SDS, at a relatively minor entropic cost. This dynamical pattern of surface "patches", including zones with low and high local concentrations of surfactant molecules, permits the existence of inner and outer solvation environments for the coumarin. Of course, as the SDS coverage approaches the full-monolayer limit, spatial surfactant distributions should become more homogeneous, local fluctuations in the density fields should drop considerably, and the dual solvation status should converge into a single one, characterized by the full embedding of the probe within the surfactant structure.

Finally, to provide an estimate for the quality of our predictions, we present results for the average values of cos θ obtained from our simulations and those reported by Benderskii et al.[23] in the second and third columns of Table 1, respectively.

TABLE 1: Solvation Parameters for Interfacial Solvation of Coumarin 314

ρ_s (Å^{-2})	state	$\langle \cos \theta \rangle$	$\omega_r^{-1/2}$ (ps)	τ_r (ps)	τ_s (ps)
0.0		0.15	0.17^a	0.35	11.9	0.80
	A	0.19		0.37	8.4	0.75
0.002	B	0.54	0.42^a	0.52	29.7	b
	A	0.37		0.38	25.6	0.83
0.005	B	0.54	0.50^a	0.44	45.3	b
	A	0.52		0.42	30.3	0.84
0.01	B	0.72	0.71^a	0.34	46.6	b

^{a} From ref 23. ^{b} Error bars are exceedingly large to provide physically meaningful values.
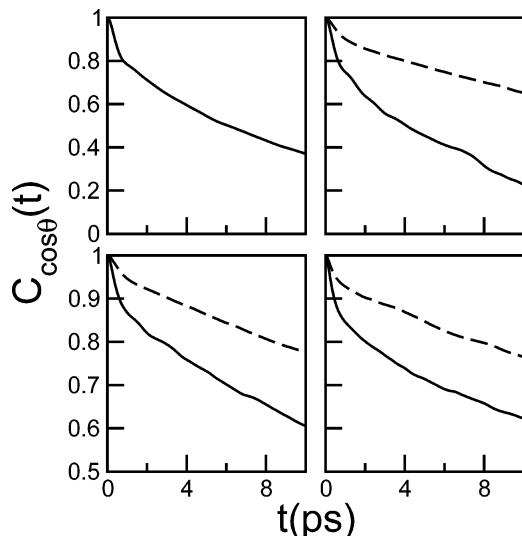

Figure 8. Time correlation function for the out-of-plane dynamics of Coumarin 314 adsorbed at charged interfaces. Top-left panel, bare interface; top-right panel, $\rho_s = 0.002$ Å^{-2}; bottom-left panel, $\rho_s = 0.005$ Å^{-2}; bottom-right panel, $\rho_s = 0.01$ Å^{-2}. Results for solvation states A (B) are shown in solid (dashed) lines.

Note that, in all cases, the experimental values from SHG experiments are intermediate between the simulated values for the A and B environments, which adds support to the solvation dynamics picture presented below.

C. Dynamical Results. The occurrence of two interfacial solvation states also has consequences in the solvation dynamics. Our analysis is based on an equilibrium time-correlation function approach and includes dynamical aspects of both the motions of the adsorbed probe and the solvation response of the interface to a change in the electronic state of the dye. For the adsorbed probe, we computed time correlations for the out-of-plane motion. The quantity of interest is

$$C_{\cos\theta}(t) = \frac{\langle \delta[\cos \theta(t)]\delta[\cos \theta(0)]\rangle_{\mathscr{O}}}{\langle (\delta[\cos \theta])^2 \rangle_{\mathscr{O}}} \qquad (5)$$

where $\delta[\cos \theta(t)] = \cos \theta(t) - \langle \cos \theta \rangle_{\mathscr{O}}$. Results for $C_{\cos\theta}(t)$ are shown in Figure 8. All plots present similar characteristics. During the first picosecond, the decays present Gaussian-like profiles and account for 10−20% of the total relaxation. This regime is followed by a much slower one, which, for all ρ_s considered, can be reasonably well-approximated by single exponentials with characteristic times τ_r. Results for the characteristic rotational time scales are presented in the fifth and sixth columns of Table 1. These were obtained assuming that $C_{\cos\theta}(t)$ can be written as

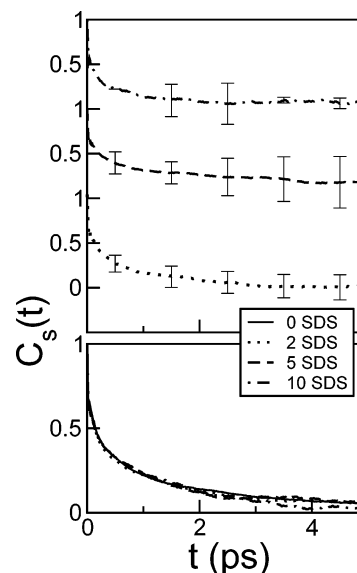$$C_{\cos\theta}(t) \approx A\,e^{-(1/2)\omega_r^2 t^2} + (1 - A)\,e^{-t/\tau_r} \qquad (6)$$

Figure 9. Equilibrium time correlation functions for the solvent energy gap for solvation states A (bottom panel) and B (top panel) at different surfactant concentrations.

Note that the presence of the surfactant does not affect the free rotational times $\omega_r^{-1/2}$ which, in turn, are between 1 and 2 orders of magnitude smaller than the molecular reorientation times τ_r. In addition, the computed τ_r values are considerably longer for states B compared to those of A, suggesting that the dynamical hindrance imposed by the surfactant is stronger in the former. Of course, the difference between these characteristic times, expressed for example in terms of the ratio $\tau_r^{\mathscr{B}}/\tau_r^{\mathscr{A}}$, decreases from ~3.5 down to ~1.5, as one moves to larger surfactant concentrations, where the distinction between solvation states A and B should progressively disappear.

To analyze the solvation dynamics at the interface, we focus on time-correlation functions for the energy gap[45] derived from the interactions of the dye with the solvent, counterions, and surfactant molecules, namely

$$C_s(t) = \frac{\langle \delta[\Delta E(t)]\delta[\Delta E(0)]\rangle_{\mathscr{O}}}{\langle (\delta[\Delta E])^2 \rangle_{\mathscr{O}}} \qquad (7)$$

The energy gap $\Delta E(t)$ is defined as

$$\Delta E(t) = \sum_{\alpha} \Delta q_\alpha V_\alpha(t) \qquad (8)$$

where Δq_α denotes the change in the partial charge of site α in the C314 as the dye is electronically excited and V_α represents the Coulomb potential exerted by the solvent, the surfactant heads, and the counterions on the tagged site. An analysis based on the linear response theory[45] is justified by the fact that, for clean interfaces, our previous studies found good agreement between $C_s(t)$ and the solvation dynamics response function obtained from full nonequilibrium simulations.[30]

Results for $C_s(t)$ for solvation states of type A are shown in the bottom panel of Figure 9. One observes that all interfaces present similar dynamical characteristics, regardless of the surfactant content. The corresponding overall solvation times obtained from the time integrals of $C_s(t)$ are in the range of $\tau_s \approx 0.8-0.9$ ps (see also entries in the seventh column of Table 1). This behavior can be interpreted by considering that (i) the solvation responses are essentially governed by molecules in close contact with the probe, which, for states of type A, would

Solvation of Coumarin 314 at Water/Air Interfaces

J. Phys. Chem. B, Vol. 109, No. 15, 2005 **7371**

mainly correspond to interfacial water with practically no contact with surfactant molecules and (ii) the persistence of large contact areas between the probe and the aqueous interface, despite the modifications in the overall orientation of the probe with respect to the z-axis.

The analysis of the dynamical responses of the interfaces for solvation states of type $\mathscr{B}$ is much more complex. The correlation functions for these cases are shown in the top panel of Figure 9. Given the magnitude of the error bars, it is evident that our attempts to extract characteristic time scales from these plots were hampered by poor statistics. Although the reasons for this failure still remain somewhat obscure to us, we tend to believe that they can be ascribed to the wide variety of relevant time scales involved in the interfacial dynamical response. Note that, in these solvation states, in addition to the dynamical modes of the water substrate and surfactant (normally characterized by time scales of the order of a few picoseconds), the overall solvation response is also indirectly modulated by the dynamical modes of the probe itself, which are typically 1 or 2 orders of magnitude slower. Moreover, we would like to point out that the distinctions between states of type $\mathscr{A}$ and $\mathscr{B}$, clearly established in terms of the behaviors of the order parameters $\cos \theta(t)$ (Figure 4) or $V_{LJ}(t)$ (Figure 6), become much more ambiguous if one wishes to discriminate solvation states based on the time evolution of $\Delta E(t)$ (not shown). In fact, the latter can be pictured as a sequence of episodes taking place at a variety of time intervals, ranging from 2−5 ps up to even a few hundreds of picoseconds, during which $\Delta E(t)$ fluctuates around well-differentiated mean values. Although we failed to correlate these episodes with changes in the order parameters $\cos \theta(t)$ or $V_{LJ}(t)$ in a clear manner, we could establish a correspondence with global changes in shape and size. Therefore, to explore the manifold of relevant time scales that dictate the dynamical evolution of the solvation—covering practically from the picosecond up to several nanoseconds—much longer simulations and elaborate analysis would be required, something that we will postpone to a future study.

IV. Conclusions

The computer simulations presented in this paper demonstrate that the addition of ionic surfactants, even at low coverages, affect the solvation of adsorbed dyes at water/air interfaces in a sensible fashion. The presence of two, well-differentiated, interfacial environments is one key feature of our results. These states can be reasonably well-discriminated by monitoring appropriate structural and energetic order parameters. For the highest surfactant concentration considered, it is possible to describe $\mathscr{A}$ and $\mathscr{B}$ in terms of the position of the coumarin with respect to the surfactant spatial domains. This dual solvation status is the result of large surfactant concentration fluctuations that prevail at low coverages, a regime that is normally referred to as the "two-dimensional gas−liquid coexistence" region.[46] Not surprisingly, we came across similar difficulties to those usually encountered whenever one intends to characterize—via computer simulation experiments—equilibrium and dynamical aspects of density fluctuations in the gas−liquid coexistence region of ordinary fluids. Under these circumstances, the appropriate sampling of the wide variety of relevant length and time scales normally requires collecting statistics of prohibitively large systems during long time spans. In the present context, we do not discard that due to finite size effects, our quantitative estimates may be affected by a nonnegligible degree of uncertainty. These effects should be more pronounced at the lowest coverage, where the amount of surfactant reduces to only

two molecules. As such, the agreement between the simulated and the experimental data for the probe orientation shown in Table 1 for $\rho_s = 0.002$ Å^{-2} may be fortuitous.

We have verified that the presence of the surfactant modifies the reorientational correlations of the probe compared to those found at clean interfaces. As a result, the distribution for the dipolar orientation of the C314 becomes narrower and gradually shifts toward more parallel alignments of the dipole with respect to the surface normal. Two reasons can be invoked to account for the latter feature: (i) for states of type $\mathscr{A}$, the enhancement of the roughness of the interface and the persistence of large contact areas between the dye and the aqueous phase; (ii) for solvation states of type $\mathscr{B}$, the competition for contact with the aqueous substrate between the dye and the surfactant polar headgroups. In passing, we also note that a similar analysis, focused on the modifications of the localization of the probe at the interface, shows less marked surfactant effects.

Our simulations also provide dynamical information related to the solvation of the dye. The presence of surfactant leads to a gradual slowing down of the probe's reorientational motion, most likely due to the interactions with the surrounding surfactants. The solvation dynamics for states $\mathscr{A}$ are little affected by the degree of surfactant surface coverage and present a characteristic time scale close to ∼0.8 ps. The solvation dynamics for states of type $\mathscr{B}$, however, turned out to be much more complex and apparently governed by a rich variety of dynamical mechanisms, which would require further work to be fully understood. Nevertheless, our results suggest that the dynamics of density fluctuations of the surfactant domains and the motions of the probe itself are key elements in the correct interpretation of the solvation responses of these charged interfacial systems.

Given the present status of our investigations, we can think of several important unanswered questions whose elucidation will lead to a more comprehensive picture of solvation at charged interfaces. First, one should still concentrate on the nature of the two-dimensional surfactant spatial domains in absence of the dye. More specifically, a detailed analysis of the size and shape distributions of the domains will surely be necessary, along with an evaluation of the time scales governing the interconversions between them. Equally important will be the analysis of the relative stabilization of dyes in each solvation environment. Finally, we want to mention the extension of the present study into the full-monolayer regime, which is currently being carried out in our laboratory. We are confident that these investigations will open new and interesting perspectives of the solvation of probes localized at more complex biointerfaces.

References and Notes

(1) References 2 and 3 provide recent review articles on chemical reactivity at interfaces and nonuniform environments.

(2) Benjamin, I. *Acc. Chem. Res.* **1995**, *28*, 233. Benjamin, I. *Chem. Rev.* **1996**, *96*, 1449. Benjamin, I. *Annu. Rev. Phys. Chem.* **1997**, *48*, 407.

(3) Nandi, N.; Bhattacharyya, K.; Bagchi, B. *Chem. Rev.* **2000**, *100*, 2013.

(4) Smart, J. L.; McCammon, J. A. *J. Am. Chem. Soc.* **1996**, *118*, 2283. Wang, H.; Zhao, X.; Eisenthal, K. B. *J. Phys. Chem. B* **2000**, *104*, 8855.

(5) Benjamin, I.; Pohorile, A. *J. Chem. Phys.* **1993**, *98*, 236.

(6) Xiao, X.; Vogel, V.; Shen, Y. R.; Marowsky, G. *J. Chem. Phys.* **1991**, *94*, 2315.

(7) Walker, G. C.; Harzeb, W.; Kang, T. J.; Johnson, A. W.; Barbara, P. F. *J. Opt. Soc. Am. B* **1990**, *369*, 1521. Jimenez, R.; Fleming, G.; Kumar, P.; Maroncelli, M. *Nature* **1994**, *369*, 471.

(8) Reynolds, L.; Gardecki, J. A.; Frankland, S. J. V.; Horng, M. L.; Maroncelli, M. *J. Phys. Chem.* **1996**, *100*, 10337.

(9) Pryor, B. A.; Palmer, P. M.; Andrews, P. M.; Berger, M. B.; Topp, M. R. *J. Phys. Chem. A* **1998**, *102*, 3284. Palmer, P. M.; Chen, Y.; Topp, M. R. *Chem. Phys. Lett.* **2000**, *318*, 440. Palmer, P. M.; Chen, Y.; Topp, M. R. *Chem. Phys. Lett.* **2000**, *321*, 62.

(10) Tamashiro, A.; Rodriguez, J.; Laria, D. *J. Phys. Chem. A* **2002**, *106*, 215.

(11) Sakar, N.; Datta, A.; Das, S.; Bhattacharyya, K. *J. Phys. Chem.* **1996**, *100*, 15483. Datta, A.; Pal, S. K.; Mandal, D.; Bhattacharyya, K. *J. Phys. Chem. B* **1998**, *102*, 6114. Datta, A.; Pal, S. K.; Mandal, D.; Bhattacharyya, K. *J. Phys. Chem.* **1996**, *100*, 10523. Rau, B. B.; Costa, S. M. B. *J. Phys. Chem. B* **1999**, *103*, 4309. Shirota, H. J. Horie, K. *J. Phys. Chem. B* **1999**, *103*, 1437.

(12) Eisenthal, K. *Annu. Rev. Phys. Chem.* **1992**, *43*, 627.

(13) Goh, M. C.; Hicks, J. M.; Kemnitz, K.; Pinto, G. R.; Heinz, T. F.; Eisenthal, K. B.; Bhattacharyya, K. *J. Phys. Chem.* **1988**, *92*, 5074.

(14) Zimdars, D.; Dadap, J. I.; Eisenthal, K. B.; Heinz, T. F. *Chem. Phys. Lett.* **1999**, *301*, 112.

(15) Zimdars, D.; Dadap, J. I.; Eisenthal, K. B.; Heinz, T. F. *J. Phys. Chem. B.* **1999**, *103*, 3425.

(16) Zimdars, D.; Eisenthal, K. B. *J. Phys. Chem. A* **1999**, *103*, 10567.

(17) Zimdars, D.; Eisenthal, K. B. *J. Phys. Chem. B.* **2001**, *105*, 3393.

(18) Benderskii, A. V.; Eisenthal, K. B. *J. Phys. Chem. B*. **2000**, *103*, 11723. Benderskii, A. V.; Eisenthal, K. B. *J. Phys. Chem. B.* **2001**, *105*, 6698.

(19) Bessho, K.; Uchida, T.; Yamaguchi, A.; Shioya, T.; Teramae, N. *Chem. Phys. Lett.* **1997**, *264*, 381.

(20) Yanagimachi, M.; Tamai, N.; Masuhara, H. *Chem. Phys. Lett.* **1992**, *200*, 469.

(21) Pant, D.; Levinger, N. E. *Chem. Phys. Lett.* **1998**, *292*, 200. Pant, D.; Levinger, N. E. *J. Phys. Chem. B* **1999**, *103*, 7846.

(22) Martins, L. R.; Skaf, M. S.; Ladanyi, B. M. *J. Phys. Chem. B* **2004**, *108*, 19687.

(23) Benderskii, A. V.; Eisenthal, K. B. *J. Phys. Chem. A* **2002**, *106*, 7482.

(24) Schweighofer, K. J.; Essman, U.; Berkowitz, M. *J. Phys. Chem. B* **1997**, *101*, 3793.

(25) Dominguez, H.; Berkowitz, M. L. *J. Phys. Chem. B* **2000**, *104*, 5302.

(26) Pohorile, A.; Benjamin, I. *J. Phys. Chem.* **1993**, *97*, 2664. Tarek, M.; Tobias, D. J.; Klein, M. L. *J. Phys. Chem.* **1995**, *99*, 1393. Bocker, J.; Schlenkrich, M.; Bopp, P.; Brickmann, J. *J. Phys. Chem.* **1992**, *96*, 9915.

(27) Conboy, J. C.; Messmer, M. C.; Richmond, G. *J. Phys. Chem.* **1996**, *100*, 7617.

(28) Carlström, G.; Halle, B. *Langmuir* **1988**, *4*, 1346. Hauser, H.; Haering, G.; Pande, A.; Luisi, P. L. *J. Phys. Chem.* **1989**, *93*, 7869. Zinsli, P. E. *J. Phys. Chem.* **1979**, *83*, 3223. Wong, M.; Thomas, J. K.; Nowak, T. *J. Am. Chem. Soc.* **1997** , *99*, 4730.

(29) Shen, Y. R. *The Principles of Nonlinear Optics*; Wiley: New York, 1984. Shen, Y. R. *Annu. Rev. Phys. Chem.* **1989**, *40*, 327. T. F. Heinz In *Nonlinear Surface Electromagnetic Phenomena*; Ponath, H., Stegeman, G., Eds.; Elsevier: Amsterdam, 1991. Bervet, P. F., Girault, H. H. *Second Harmonic Generation at Liquid/Liquid Interfaces*; CRC Press: Boca Raton, FL, 1996. Eisenthal, K. B. *Acc. Chem. Res.* **1993**, *26*, 636.

(30) Pantano, D. A.; Laria, D. *J. Phys. Chem. B* **2003**, *107*, 297.

(31) In absence of surface active dyes, the density of the saturated SDS monolayer rises up to $\sim 2 \times 10^{-2}$ Å^{-2}.

(32) Berendsen, H. J. C.; Postma, J. P. M.; Von Gunsteren, W. F.; Hermans, J. *Intermolecular Forces*; Reidel: Dordrecht, 1981.

(33) Liotard, D. A.; Healey, E. F.; Ruiz, J. M.; Dewar, M. J. S. *QPCE Bull.* **1989**, *9*, 123. *AMPAC*, version 2.1i; Quantum Chemistry Program Exchange; Program No. 506.

(34) McCarthy, P. K.; Blanchard, G. J. *J. Phys. Chem.* **1993**, *97*, 12205.

(35) Rechthaler, K.; Köhler, G. *Chem. Phys.* **1994**, *189*, 99.

(36) A similar parametrization to that used in the present study was employed in ref 30.

(37) Moylan, C. R. *J. Phys. Chem.* **1994**, *98*, 13513.

(38) Allen M. P.; Tildesley, D. J. *Computer Simulation of Liquids*; Clarendon: Oxford, 1987.

(39) Although the implementation of Ewald summation techniques and variants thereof (see refs 40 and 41) is known to provide more accurate descriptions for the electrostatics of periodically replicated systems in two dimensions, solvation dynamics results seem to be only mildly affected by the truncation of long-range forces, an approximation that introduces a considerable savings in computational effort. See ref 42.

(40) Essmann, U.; Parera, L.; Berkowitz, M. L.; Darden, T.; Lee, H.; Pedersen, J. G. *J. Chem. Phys.* **1995**, *103*, 8577. Yeh, I.-C.; Berkowitz, M. L. *J. Chem. Phys.* **1999**, *111*, 3155.

(41) Feller, S. E.; Pastor, R. W.; Rojnucharin, A.; Bogusz, S.; Brooks, B. R. *J. Phys. Chem.* **1996**, *100*, 17011.

(42) Vieceli J.; Benjamin, I. *J. Phys. Chem. B* **2003**, *107*, 4801. Vieceli J.; Benjamin, I. *J. Phys. Chem. B* **2002**, *106*, 7898.

(43) Jungwirth, P.; Tobias, D. *J. Phys. Chem. B* **2000**, *104*, 7702. Jungwirth, P.; Tobias, D. *J. Phys. Chem. B* **2001**, *105*, 10468.

(44) The local coordinate system reported in ref 15 is slightly different from that adopted here. In particular, $\cos \theta$ is measured with respect to the ζ direction, taken along the molecular transition dipole moment. Still, we believe that this difference should not preclude a direct comparison between simulation and SHG results.

(45) Carter, E. A.; Hynes, J. T. *J. Chem. Phys.* **1991**, *94*, 5961. See also Chandler, D. *An Introduction to Modern Statistical Mechanics*; Oxford University Press: New York, 1987. Chapter 8.

(46) Gaines, F. L., Jr. *Insoluble Monolayers at Liquid−Gas Interfaces*; J. Wiley & Sons: New York, 1966.